USNC-Tech

Trade Study of Different Nuclear Power Architectures to Sustain a Commercial Lunar Base

Jonathan Giovannacci

Marina Ruiz Izu

Max Monange

2022

Master's of Engineering Capstone Project

UC Berkeley Department of Nuclear Engineering

Contents

List of Figures

List of Tables

1 Executive Summary

In partnership with Ultra Safe Nuclear Corporation (USNC), this trade study aims to analyze the optimal solutions based on best available technology to develop a power transport architecture for a small commercial lunar base powered by a nuclear reactor. Energy will be provided by the Pylon reactor [1], a 150 KWe High-Temperature-Gas-Cooled Micro Reactor provided by USNC. The first part of the report will focus on context and an industry analysis of the power requirements for a commercial lunar base, while the second part will analyze the proposed solutions for power transfer to utilities. The operations that are envisioned are Hydrogen and Oxygen production, water production and Environmental control and life support system. These utilities will be key for both the commercialization of the lunar base and sustenance of human life. Hydrogen and Oxygen production are key to produce rocket fuel, allowing for the moon to become a refueling outpost for rockets aimed at Mars or deep space, kick-starting a new age of exploration and potentially asteroid mining. The main item of the trade study will be analyzing high temperature heat transfer to the utilities, for which three main technologies are being envisioned: Liquid metal or molten salt, as a solution that uses a liquid coolant, Helium or Carbon Dioxide, as a gas coolant heat transfer solution and a fully electric solution, which will not involve any thermodynamic heat transfer at all.

2 Context: Lunar Outpost Power Requirements

2.1 Environmental Control and Life Support Systems (ECLSSs)

The habitat is a closed infrastructure in the base camp able to support personnel and equipment. The main power demand (P_{ls}) for the habitat will come from the environmental control and life support systems (ECLSSs) which consists of the following life support activities:

- Air handling and conditioning (CO2 removal, oxygen transport).
- Habitat heating
- Habitat cooling
- Biomass
- Food storage processing
- Waste processing
- Water processing
- Extravehicular activity support

Per request from USNC, the first two ECLSSs listed above will be explored in more details in section 2.1.1 and 2.1.2.
The power requirements for the remaining systems are taken from NASA estimations [2] and listed in the table below.

ECCLSS	**Power required [kW]**
Air handling ($P_{\mathbf{ahc}}$)	5.85
Biomass ($P_{\mathbf{biomass}}$)	6.10
Food ($P_{\mathbf{food}}$)	4.27
Thermal Cooling ($P_{\mathbf{cool}}$)	1.03
Waste processing ($P_{\mathbf{food}}$)	0.01
Water processing ($P_{\mathbf{water}}$)	1.29
Support for extravehicular activities ($P_{\mathbf{eva}}$)	2.50
Total ($P_{\mathbf{ls}}$)	21.05

Table 1: Repartition of ECLSS power requirements

One can note that heating power is not included. It will be shown in section 2.1.2 that heating requirements can be compensated by waste heat from ECLSS.

2.1.1 Air Handling and Conditioning: CO2 Removal and O2 Generation

Similar to the technology on the International Space Station (ISS), the air handling system in the lunar habitat uses regenerable carbon dioxide removal equipment based on molecular sieve [3], a material with pores of uniform size. The technology is a four-bed molecular sieve. The bed absorbs carbon dioxide which is dissociated from the absorbing media and exhausted from the habitat without recovering any of the extracted molecules. The four-bed molecular sieve uses the principal of adsorption in order to selectively remove CO2. Air can be purified at a rate of 54.5kg/hr [4].

On a mass basis, water vapour and CO2 are the most common contaminants inside space human habitats, but a wide range of trace organics may also be present. For the safety of the crew, these are removed by the trace contaminant control system (TCCS). TCCS for atmospheric gases uses activated carbon for non-combustible trace gas removal, and high efficiency particulate air filters for bacteria and particulate removal [3] Activated carbon is an excellent sorbent for the removal of a broad range of organic contaminants. Neither of the commodities removed are regenerated. Moreover, the TCCS also removes trace combustible gases from the crew cabin.

Oxygen and nitrogen are supplied in a pressurized gaseous form from high-pressure stores. A major constituent analyser and a fire detection and suppression system monitor for air contaminants and combustion products.

Together, the molecular sieve beds, the TCCS, oxygen nitrogen generation and detection systems consume 5.85kW of power (P_{ahc}) while operating.

2.1.2 Habitat Heat Loss

Heat loss from the habitat at night was analysed to determine whether a heater would be required to keep the infrastructure at standard ambient temperature. The quantity of heat lost through the insulation depends on the shape of habitat (which was assumed to be a hemisphere in this case), the desired habitat temperature (T_{hi}) and the nigh time outdoors heat sink temperature (T_{sn}). It is important to note that multi-layer insulation (MLI) was assumed in the analysis carried by NASA [2] since it has excellent resistance properties against heat flow. The majority of heat losses resulted from pass-through and seams in the insulation covering created by wires and tubes that travel through the insulation. The different types of heat losses were compiled in the following table.

Type of heat loss	**Amount [W]**
Heat loss from the habitat through the insulation	245
Heat leak from pass-throughs and seams in the insulation covering	1,883
Heat leak through conduction from the sources below	1,968
Heat leak from the habitat to the radiator	42
Heat loss through the support legs	426
Heat loss through the airlock structure	1.500
Total	4.096

Table 2: Human Habitat Heating heat losses

All formulae and variables are in Appendix A and B.

The heat leaks through the habitat radiator are a direct result of the coolant loop being turned off at night to minimize heat loss from the radiator. The radiator temperature drops to match the surroundings temperature since no heat flows through it anymore. Heat is lost by conduction down the coolant tubes that connect the radiator to the habitat. The same conduction mechanism causes heat loss through the support legs and the airlock structure. The cross sectional area of a conductive path is given by the expression for A_{cp} above where it is assumed that any path considered can be represented by a hollow cylinder with inner diameter d_{icp} and wall thickness d_{cp}.

It was concluded in this study that waste heat from ECLSS operation can be utilized to make up all of the heating power requirements [1]. In this case, no additional heat power P_{ht} is required since $\dot{Q}_h < P_{ls}$. However, as the habitat volume increases, heat input might be needed.

2.2 High Temperature Thermal and Chemical Processes

2.2.1 Water Production

Water extraction is a necessary process to establish a lunar base, not only is water one of the main resources for life, but it is the key element for hydrogen production. Ice is relatively abundant in lunar soil at a concentration of 5 % [5].

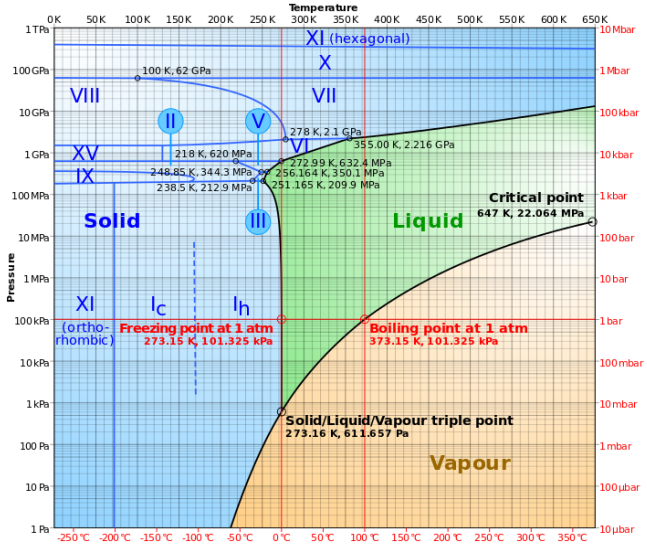

(a) Water Phase Diagram

Figure 1: Water phase diagram

The currently best envisioned method to extract water from the soil is to heat the soils at sublimation temperatures in order to produce water vapor at high temperature, roughly 648K. It requires 10KW of heating power to produce 14.78Kg of water vapor at that temperature over the extended period of time of about 8 hours and a half, or 30800 seconds to be exact, as shown in figure 2. This would result in the production of 0.48 g/s of water vapor (or 41.472 Kg/day) that can be either pressurized and condensed into liquid water or sent to undergo electrolysis to produce hydrogen and Oxygen gas. as seen in the phase diagram for water in figure 1, the low lunar pressure environment (in the order of magnitude of nanopascal), is far below the triple point of water and is optimal for water sublimation.

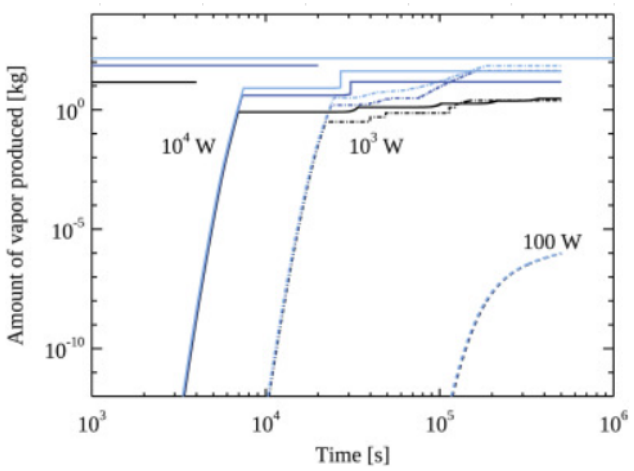

(a) Water extraction requirements

Figure 2: Thermal energy requirement for water extraction

2.2.2 Liquid Rocket Propellant Production

Oxygen Production: Hydrogen and oxygen are obtained through the hydrogen reduction of Ilmenite. Ilmenite is a mineral that consists of iron titanium oxide ($FeTiO_3$). Firstly, hydrogen gas will need to be supplied to feed the fluidized bed reactor and kick-start the reaction, then the hydrogen produced by the electrolyzer is fed back into the cycle. Once the process reaches steady state and the hydrogen produced can consistently feed the FBR, supply will stop and the process will continue as a semi-closed cycle, where only ilmenite is supplied.

Oxygen is extracted through the following process: First, ilmenite and Hydrogen react at approximately 1000^{o}C in a fluidized bed reactor (reaction 1). As products, water is formed and the next step comprises the electrolysis of water to separate it in its main components hence producing oxygen and hydrogen (reaction 2).

$$2FeTiO_3+2H_2 \rightarrow 2Fe+2TiO_2+2H_2O \quad (1)$$

$$2H_2O+ \rightarrow 2H_2+O_2 \quad (2)$$

The sequence in which oxygen is generated comprises several steps that will be discussed as follows: First, the regolith, in which ilmenite is contained, is transported to the screen; Second, A vibrating screen is used to filter out particles with larger than 1mm in diameter; Third, Ilmenite needs to be separated from the regolith in a magnetic separator; Fourth, the mineral dust is directed towards the fluidized bed reactor in which the reaction with Hydrogen will take place at high temperatures. The requirements of temperature and time are 1273K and 1h respectively; Fifth, the vapor is passed through the electrolyzer where it is separated into Oxygen and Hydrogen. Finally, Oxygen will be

stored to be used in any desired purpose on the lunar surface while Hydrogen will be fed back to the bed reactor to perpetuate the reaction.

Power requirements will be sized according to the desired oxygen production, this will determine the mass rate of ilmenite (and therefore mass rate of regolith) which needs to be fed into the system. Our power demand analysis will be limited in thermal and electrical power consumption [2]. The electrical power processes include regolith scooping and transport, vibratory screener, separation of regolith and ilmenite, ilmenite lifting, and the electrolyser. On the other hand, thermal power is specifically used for ilmenite reaction with hydrogen. The formulae used to calculate power for each activity are mentioned in appendix C. The final absolute quantification results for these processes are illustrated in 3 and 4 for electrical and thermal power respectively.

Desired oxygen rate has been calculated through an iterative method where desired particle size is obtained (d_s). The equation below determines the maximum particle size for an efficient process in the Fluidized Bed Reactor [2].

$$\frac{150\rho_{H_2}(1-\epsilon_p)U_{H_2}}{\tau^2\epsilon^3\mu_{H_2}} = \frac{g\rho_{H_2}(\rho_{ip}-\rho_{H_2})}{\mu^2_{H_2}}d_s^2 - \frac{1.75\rho^2_{H_2}U^2_{H_2}}{\tau^2\epsilon^3\mu_{H_2}}d_s \tag{3}$$

Our desired Oxygen rate has been calculated to be $2kg/h$. It is then possible to calculate how much hydrogen is needed in proportion to oxygen through reaction 1: $M_H = \frac{M_O}{32}\frac{molH_2}{molO_2}$

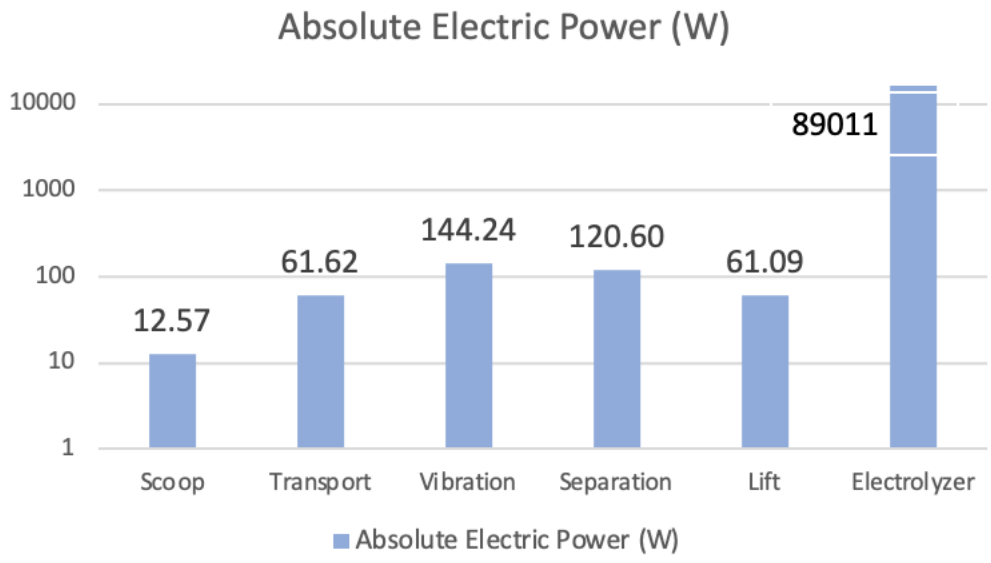

Figure 3: Electric Power

The bulk of the power is dedicated to power the electrolyzer as seen in 3 with the rest of activities requiring a smaller fraction of the power, therefore, these are neglectable in the power quantification

process.

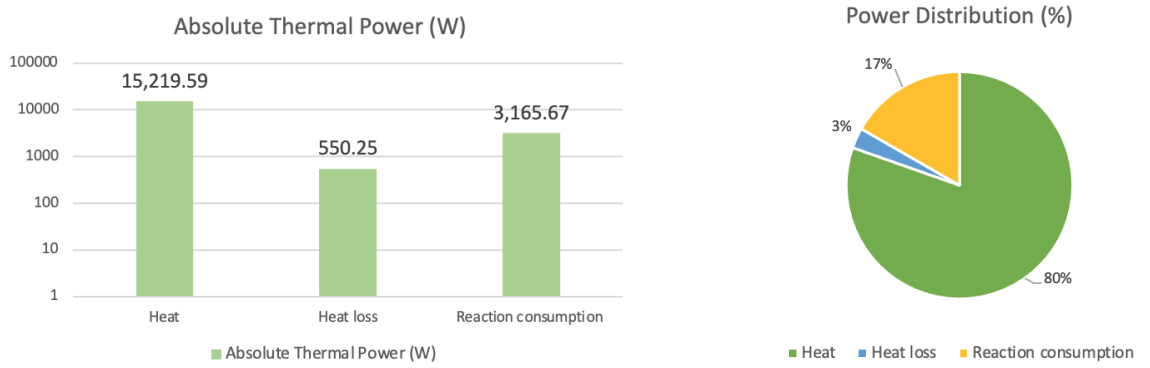

(a) Thermal Power

(b) Thermal Power Distribution

Figure 4: Thermal Power Requirements

2.2.3 Water, Oxygen, Hydrogen and Iron Extraction Process

For the FBR to produce the desired 2 kg/h of oxygen, a total mass rate of 627.3 kg/h of regolith is required. On lunar soil, water is present as ice crystals at a relatively high percentage, estimates range between 3% and 9% [6]. In the following calculations, an average of 5 % ice concentration is assumed. Water is collected through the heating of regolith at high temperatures such that ice crystals sublimate directly into water vapour. given the rate of regolith, a mass rate of 31.36kg/h of water vapor will enter the system. Half of the water is going to be stored, and half is sent to the Electrolyzer, for the separation of Hydrogen and Oxygen. A total of 15.8 kg/h of water is processed through electrolysis resulting in oxygen, hydrogen, and Iron. 12.5% of the resulting hydrogen needs to be recirculated to the FBR, while 1.74kg/h are extracted and stored.

The sizing of the processes is driven by the demand of Hydrogen and Oxygen for the rocket fuel. Depending on the needs, all processes can be scaled up in size and numbers. The overall power distribution is relatively even, with roughly a 50/50 distribution in thermal and electric energy demand.

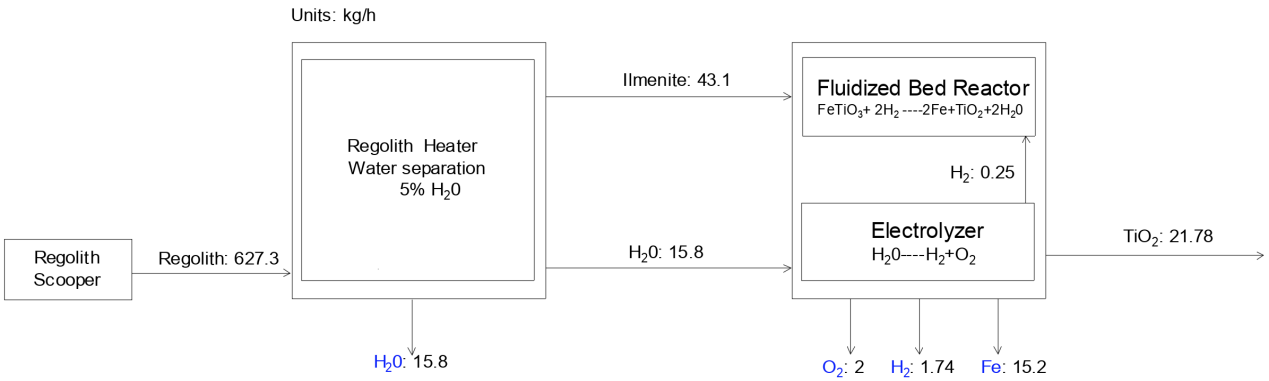

Figure 5: Flow mass rate diagram for FBR and water separator facilities

Hydrogen production is one of the key processes necessary for commercial operations in space. Hydrogen not only can be used as a fuel for some types of chemical rockets, but could allow the production of fuel cells. Currently, coupling nuclear power with hydrogen production is being envisioned on earth, as high-temperature-gas-cooled reactors, such as the pylon reactor, are capable of reaching high enough temperatures to make hydrogen production more efficient. The 2023 SOA hydrogen production technology enlists energy demands of 60kJ per mole of H_2 gas and electric demands of 180KJ per mol of Hydrogen. For 1 mol of H_2 being roughly equal to 2g, the process would require 90KJel and 30KJth per kilogram of hydrogen produced.

At peak capacity, this technology can produce up to 1000kg of Hydrogen per day or an equivalent of 11.574g/s, therefore, demanding power requirements of 2.1KWel and 0.694KWth of power.

2.3 Miscellaneous

2.3.1 Communication

To support life on the base camp, communication relays between Earth and Moon are needed for operations, as well as on the lunar surface. Three different connection links will be analyzed: Lunar-to-Earth, Lunar-to-Orbit, and Lunar Surface-to-Lunar Surface. The connection is provided through the interaction between a transmitter and a receiver station.

There are several assumptions that need to be considered. First, the transmitter and receiver tower height is 10 m in both cases. The center operating frequency is 30 GHz and the effective noise temperature needed to calculate the noise power level is 270K.

In the process of calculating the power requirements for both transmitter and receiver, the data rates for the three different connections is summarized, where the distance between the two nodes is

specified in 3 [7].

Spacecraft link to:	Data rate (Mbps)	Distance (kg)
Earth-to-Lunar surface		
Earth ground	3000	384000
Earth Orbit relay	1000	384000
Orbit-to-lunar surface		
Relay spacecraft	1000	6500
Lunar surface-to-Lunar surface		
Moon low rate	10	2700
Moon science orbiter	100	2700
Moon human outpost	1000	2700

Table 3: Data rate for communication links

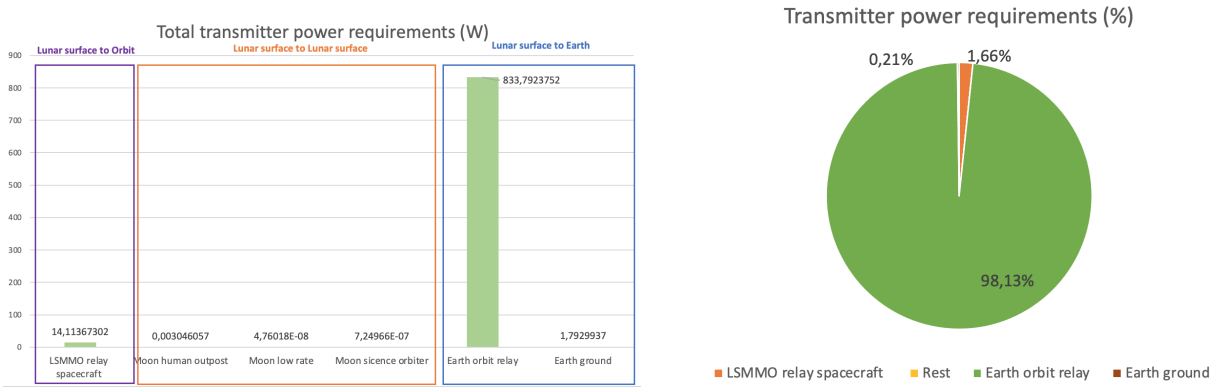

(a) Transmitter Power

(b) Transmitter Power Distribution

Figure 6: Communication Transmitter System

The bulk of the transmitter power is dedicated to the Lunar Surface-to-Earth connection orbit relay followed by the Lunar-to-Orbit relay spacecraft.

2.4 Power Requirements Summary

Power requirements are divided between thermal and electric. Most of the electric power is dedicated to O_2 and H_2 production in the electrolysis of water. An important power requirement in the electric perspective is the ECS. On the other hand, the thermal power has two main purposes water sublimation and ilmenite reaction in the FBR for O_2 and H_2 production.

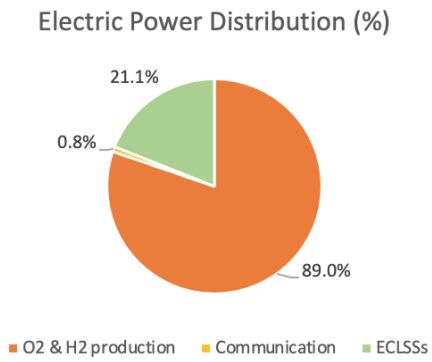

(a) Total Electrical Power Distribution

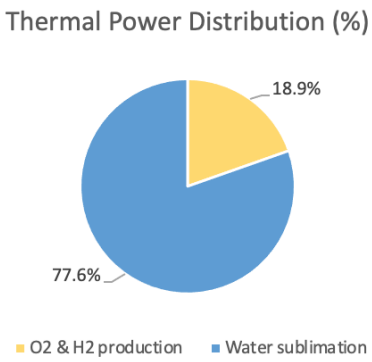

(b) Total Thermal Power Distribution

Figure 7: Total Power Distribution

3 Trade Study

In this section, the analysis of two different approaches will be addressed in regards to the means of power delivery for the power requirements previously discussed. One solution is to consider the use of a secondary loop based on fluid heat transfer to deliver the thermal power to both water sublimation and ilmenite reaction in the FBR. The study will discuss the use of four potential fluids: molten salt, sodium, helium and CO_2. In the second approach, all power requirements will be delivered in a full electric solution. The conversion from electrical to thermal power will be required to fulfill the thermal power.A Brayton cycle energy conversion will satisfy the electrical energy needs through the use of turbo-machinery technology.

3.1 Fluidic Thermal Power Transport Solution

The next diagram represents the thermodynamic cycle. The red lines depict the primary loop, which is composed of the reactor, the heat-exchanger between the first and secondary loop, the turbo-machinery (turbine and compressor), radiator, and a recuperator before the reactor. The blue lines represent one of the approaches to deliver the thermal power needs to the system. The different fluids considered for the study will deliver heat, then they will be redirected into the heat-exchanger by either a compressor or a pump, depending on the state of the fluid. Lastly, the electric generator system will generate the electricity with the generator coupled with the turbine and will be transformed with a transformer at the end point of the line to equate it to the demand voltage.

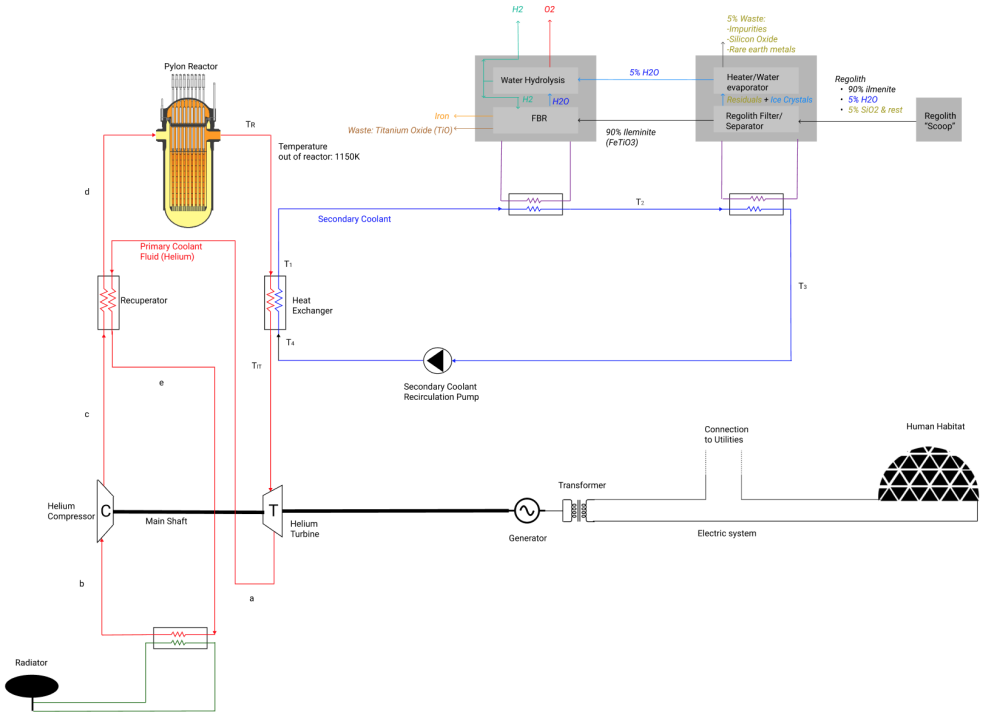

Figure 8: Energy System diagram

Temperature requirements need to be satisfied according to the type of process for the primary and secondary loop. As the reactor temperature is concerned, the maximum that the reactor can produce is 2000K (T_R). It should be noticed that in order to work with the Brayton cycle stated in [1] an inlet turbine temperature of 1150K (T_{IT}) was necessary. In the secondary loop the first utility consists of the production of oxygen and hydrogen through the use of a fluidized bed reactor which requires a minimum temperature of 1073K (T_2) as the reactor states. In the case of water sublimation, the temperature needed should stay above 648K (T_3), so a temperature of 800K is established.

3.1.1 Computational Model

Reactor Temperature Analysis: A finite element analysis model describes the fluid flow in the heat exchanger and the piping system of the secondary loop. The secondary loop's Temperatures and mass rates are obtained from power requirements and adjusted for each coolant type. The goal is to obtain the heat exchanger length, Maximum reactor temperature, pipe size and thickness for each solution.

The Fluidized Bed Reactor and water sublimation require a thermal power of 19kW and 77.5kW respectively, with temperature requirements of 1073K and 800K. Mass rate and the outlet heat ex-

changer temperature of the secondary fluid (T_1) are calculated with the equations that follow:

$$Q_{water} = \dot{m}_{fluid} Cp_{fluid} (1073K - 800K) \tag{4}$$

$$T_1 = \frac{Q_{FBR}}{\dot{m}_{fluid} * Cp_{fluid}} + 1073K \tag{5}$$

The calculated mass rates and temperatures are inserted in an iterative process, in which Heat exchanger length and peak temperature of Helium out of the pylon reactor are manipulated until the desired T_1 is reached. These process are repeated for the four potential fluid solutions in the secondary loop.

Piping Dimensional Analysis: In terms of dimensioning the secondary loop lengths and diameters of pipes will be determined for the four fluids. The piping can be divided in 4 sections: length of the heat exchanger, length for the first facility (FBR), length of the water sublimation facility and finally the length to return to the heat exchanger.

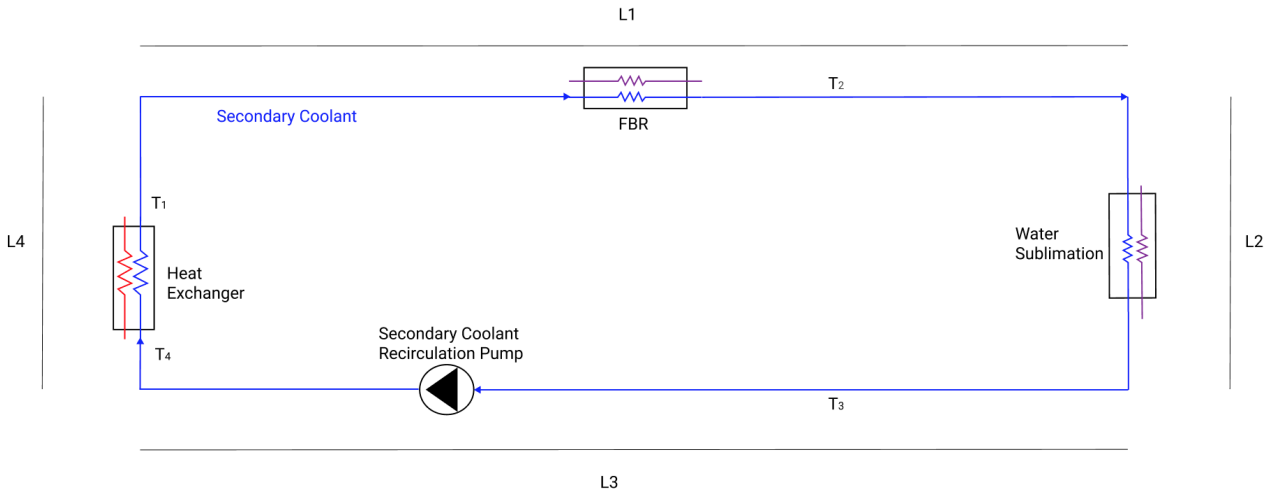

Figure 9: Secondary Loop System Diagram

The thickness of the pipes will be also determined in order to estimate the amount of piping material using the next equation.

$$t = \frac{\text{Design Pressure} * \text{Diameter}}{2 * \text{Specified Minimum Yield Strength} * \text{Longitudinal joint factor} * 0.72} \tag{6}$$

Pressure Analysis: The pressure analysis throughout the length of the secondary loop will be achieved by applying Conservation of Energy (Bernoulli Equation) in an infinitesimal section of the pipe to evaluate the pressure at each point. The equations that follow represent how an incompressible and compressible flow are modeled applying Bernoulli equation.

For incompressible flow:

$$\rho + \frac{v^2}{2} + gz = Constant \tag{7}$$

For compressible flow:

$$\int \frac{dp}{\rho} + \frac{v^2}{2} + gz = Constant \tag{8}$$

Due to the conservation of energy, as the fluid flows through the pipe there are losses caused by the friction between the material and the fluid. This friction causes head losses that can be locally generated like in elbow points, valves and pumps or throughout the length of the pipe (Find the terminology in the appendices).

$$h_L = (f(L/D) + \sum k_i)\frac{v^2}{2} \tag{9}$$

These three analyses will be applied individually for the 4 fluids in study and as a result the reactor temperature, heat exchanger length, piping dimensions (lengths and diameter) and pressure development will be determined for gases (He and CO_2) and liquids (Sodium and Molten Salt).

3.1.2 Helium and Carbon Dioxide Transport Solution

Reactor Temperature Analysis with Helium: For He-He heat exchanger the following data for mass rate and T_1 are obtained:

$\dot{m}_{fluid}$ (kg/s)	T_1 (K)
0.0547	1139.64

The combination of heat exchanger length and reactor temperature that approximates T_1 with and error of 0.26% is:

T_R (K)	HX Length (m)
1580	1

The following graph represents the heat transfer and temperature evolution along the heat exchanger length for both the primary and the secondary loop. The red line represents helium in the primary loop where the inlet temperature is the reactor temperature and the outlet temperature (1182K) is the one before entering the turbine which is close enough to the target value of 1150K. On the other side, the blue line represents helium but in the secondary loop starting with the required temperature of water sublimation and heating up through the heat exchanger until it reaches T_1 calculated by the model of 1136K.

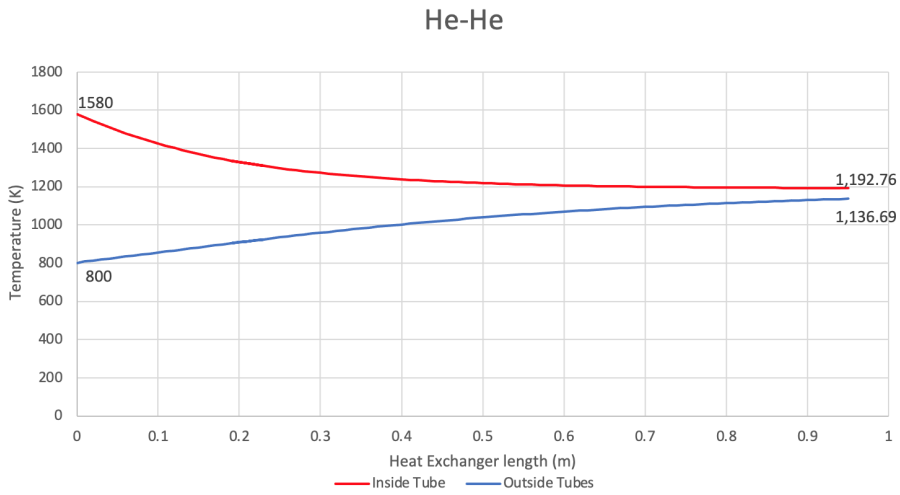

Figure 10: He-He Heat Exchanger

Reactor Temperature Analysis with CO_2: For He-CO_2 heat exchanger the following data for mass rate and T_1 are obtained:

$\dot{m}_{fluid}$ (kg/s)	T_1 (K)
0.2822	1139.64

The combination of heat exchanger length and reactor temperature that approximates T_1 with and error of 0.23% is:

T_R (K)	HX Length (m)
1600	5.5

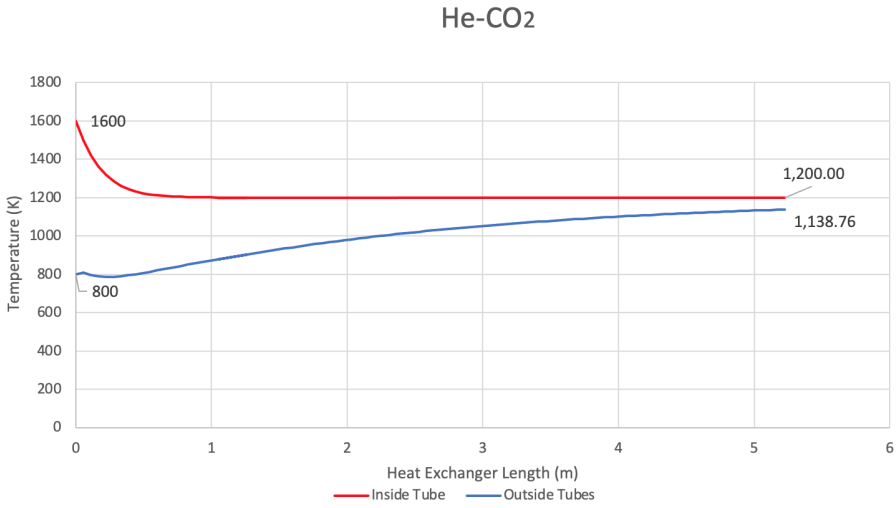

Figure 11: He-C0$_2$ Heat Exchanger

In the gas transport solution, He-He is a viable solution since it requires a reactor temperature of 1560K which is below the threshold of 2000K. From a manufacturing point of view the 1 m length heat exchanger can also be easily manufactured. Also, as can be inferred from the data in the CO_2 solution, the pour heat conductivity of CO_2 requires the enlargement of the heat exchanger to 5 m as well as a high reactor temperature of 1600K. Therefore, it was concluded that He is more viable solution for the thermal transport solution since it requires smaller dimensions to enable the heat transfer needed and a lower demand from the reactor output temperature.

Piping Dimensional Analysis: In order to find the diameter, conservation of mass will be applied using the mass rate imposed by the thermodynamic cycle. The mass rate can be associated with the diameter through velocity and area: $\mathrm{m} = \rho Q = \rho v \pi \frac{D^2}{4}$ In order to establish a value for the velocity of the fluid, the extreme case of supersonic velocity was considered so the minimum diameter can be found. The supersonic velocity is calculated as the average supersonic velocity throughout the heat exchanger by applying:

$$a = \sqrt{\frac{C_p RT}{C_v M}} \tag{10}$$

Therefore, the final minimum diameter is calculated as: $D_{min} = \sqrt{\frac{4 * \dot{m}/\rho}{a\pi}}$

In the following table, the length for the 4 different sections as well as the pipe diameter for the two fluid solutions are summarised. As the fluid should stay in the sub-sonic region, the diameter will be doubled to ensure that super-sonic conditions. Equation 6 can be used to calculate the thickness of the tubes.

Fluid	$L_1(m)$	$L_2(m)$	$L_3(m)$	$L_4(m)$	$D_{min}(m)$	$D_{tube}(m)$	Thickness (mm)
He	0.8	1	0.8	1	0.058	0.1167	3.5
CO_2	0.8	5.5	0.8	5.5	0.1623	0.3246	7.1

Figure 12: Piping dimensions for the gas transport solution

A greater diameter is obtained for CO_2 than for He.

Pressure Analysis with Helium: The secondary loop using Helium will use a pressure of 15 bar in the heat exchanger. Throughout length L1 the pressure arises from 15 bar to 15.18 bar representing a 6% increment. In the second section L2 the pressure keeps arising but with a higher increase of 30%. These two sections experience a rise in pressure due to the heat transfer which leads to an increase in density as the temperature decreases linearly. Lastly, in the section L3 there is no exchange of heat so the friction of the fluid with the piping leads to a loss of pressure of 0.001%. The maximum pressure that is reached is 18.9 bar representing an increase of 26%. The total pressure difference between the two extremes of the pipe is 3.4 bar. Therefore, one possible solution to reduce the pressure is to use relief valves.

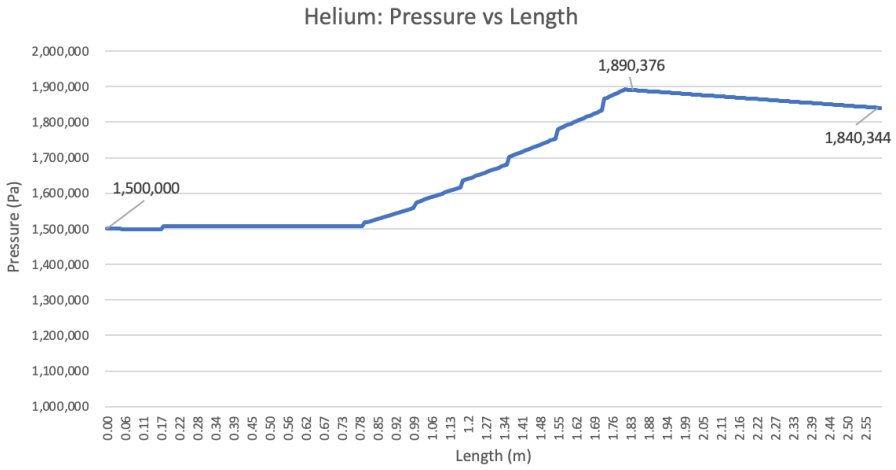

Figure 13: He Pressure (Pa) throughout secondary loop

Pressure Analysis with CO_2: Starting with a pressure of 10 bar, throughout length L1 the pressure arises 4%. In the second section L2 the pressure keeps arising but with a higher increase of 28%. Similar to the Helium case, these two sections experience a rise in pressure due to the heat transfer leading to an increase in density as the temperature decreases linearly. Lastly, in the section L3 there is no exchange of heat so the friction of the fluid with the piping leads to a loss of pressure of

1%. The final pressure obtained is 13.42 bar being an increment of 32%. The difference between the initial and final pressure is 3.28 bar. Similar to He, it is necessary to use a mechanism that enables to reduce the pressure, therefore, a relief valve is suggested as a potential solution.

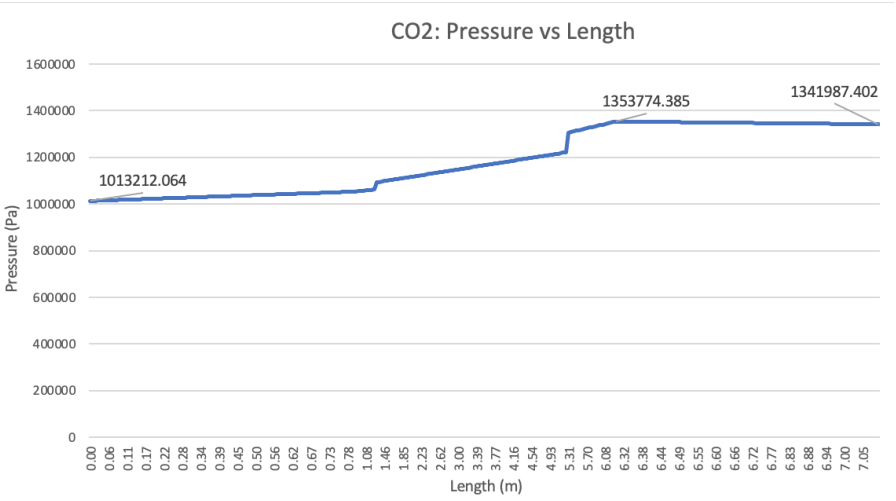

Figure 14: CO_2 Pressure (Pa) throughout secondary loop

3.1.3 Molten Salt and Liquid Sodium

The choice of analyzing heat transfer through these two mediums is mainly driven by the harsh atmospheric conditions on the lunar surface and excellent thermal properties of the two fluids. In addition, both Nuclear and Solar research has been key for recent development of Liquid Sodium and Molten Salt heat transfer technologies, hence it could be reasonably expected that in the time frame of the next lunar landing, these technologies will be available and possibly even adopted on earth. The Molten Salt chosen for this scope is a baseline mixture of the following Chloride salts: NaCl, KCl, and MgCl. Both Molten Chloride and Sodium benefit from high heat capacity, heat transfer coefficients and high boiling points, well fitting for the high temperature and low pressure operations on the moon[8].

The values obtained for mass rate and T1 are:

$\dot{m}_{fluid}$ (kg/s)	T_1 (K)
0.2715	1140.813

For Molten Chloride, and

$\dot{m}_{fluid}$ (kg/s)	T_1 (K)
0.2232	1139.44

For Sodium, which correspond to the following values of Reactor Temperature and Heat Exchanger

Length:

Fluid	T_R (K)	HX Length (m)
Molten Salt	1570	10
Sodium	1490	0.5

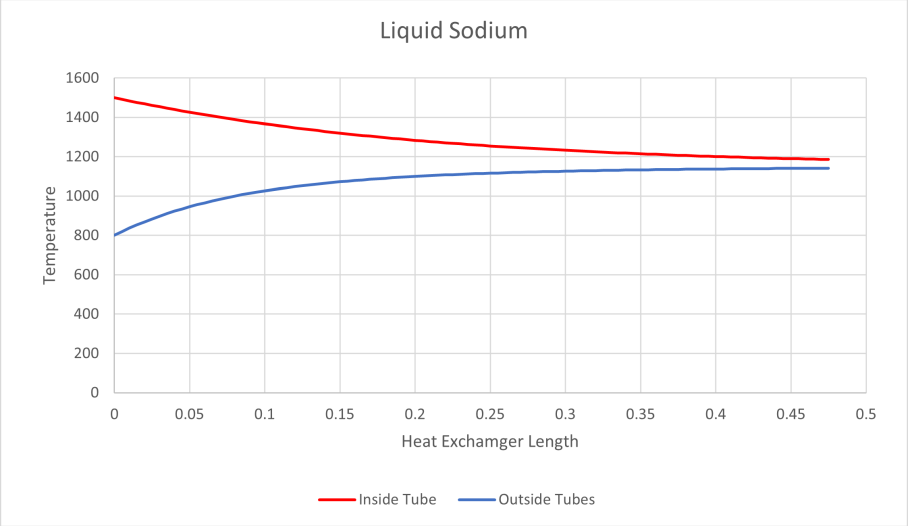

Figure 15: Helium - Liquid Sodium Heat Ex-changer

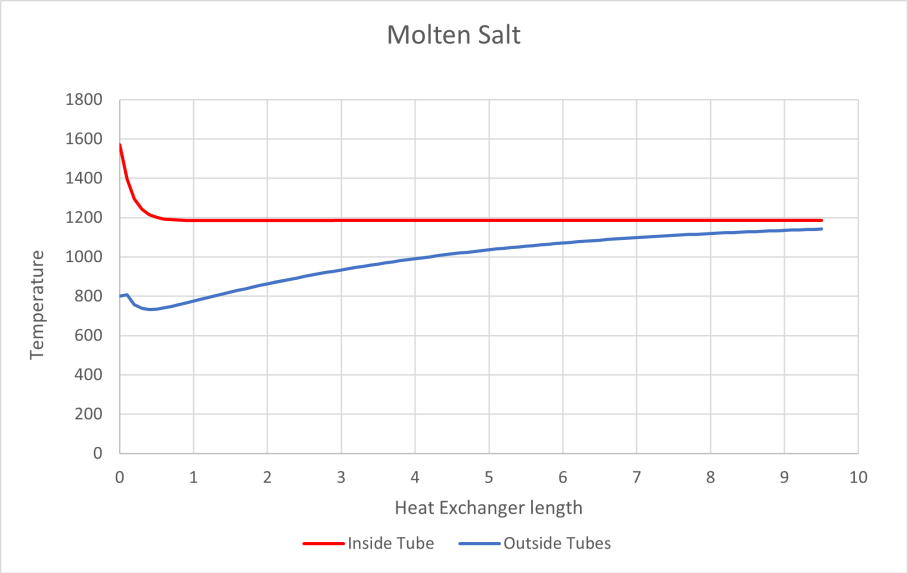

Figure 16: Helium - Molten Chloride Heat Ex-changer

Notably, liquid sodium provides good results for reactor temperature and size of heat ex-changer, while molten salt requires larger parameters. The low mass rates are good for design of recirculating

pumps, but due to high viscosity, molten salt requires smaller pipes to achieve turbulent motion. This could prove to be a technological complication in system design. It is also important to note that all available data has been measured in different conditions in comparison to the lunar parameter and may not be accurate as a result. There is a need for more literature on operation of these fluids at low pressure and high temperature. [9].

A recirculating pump might need to be implemented in the system, as the velocity of the fluids will decrease through the cycle. the difference in velocity is respectively 0.039 m/s for molten salt and 0.0024 m/s for liquid sodium. These small velocity changes could be compensated with pipe geometry or height to allow natural circulation, given the small values, but these results do not take into account chemical properties, and accurate 3D fluid analyses that may change the overall results. There is a need for more real testing.

Pipe Sizing One of the greatest properties of utilizing these liquid coolants for heat transfer is the working pressure. The main limitation in pressure is due to the boiling point of the liquids. It is important that the fluids are kept above vapor pressure in order to avoid the formation of bubbles in the coolant, both to avoid cavitation in the turbomachinery and to avoid localized temperature peaks. For the two fluids, Vapor pressure is calculated through experimental equations at max temperature and are equal to 39.092 kPa for molten chloride and 88.705 kPa for sodium. This highlights one of the greatest characteristics for molten salt for a heat transfer fluid in the lunar environment, which is the relatively low pressure needed to carry out heat transfer at high temperature.

Equation 6 can be utilized to calculate the thickness of stainless steel pipes, but the results show a very small thickness of 3.42 micron for molten salt and 35.9 micron for sodium. These results, while technically promising as they show that the construction materials have very low chance of failure from the pressure, are not realistic in terms of design of pipes due to considerations towards structural integrity. A value of 2 mm thickness will be then chosen for the pipe size.

3.2 Mass Results

The mass requirements accounts for the mass fuel required for each fluid solution. The total mass is calculated based on the volume of the secondary loop given the dimensions of lengths (L1, L2, L3, L4) and diameter of the tube assembly.

$$\text{Coolant mass} = \overline{\rho}\text{Volume} = \overline{\rho}[\ (\frac{\pi D_{tube}^2}{4} * (L1 + L2 + L3)) + (\frac{\pi D_{HX}^2}{4} * L4)] \tag{11}$$

Fluid	Average Density (kg/m^3)	Total Volume (L)	Mass (kg)
He	0.7537	27.88	0.021
CO_2	5.72	588	3.363
Na	763.02	25.604	19.536
Molten Salt	1556.64	12.49	19.447

Figure 17: Fluid Mass Results

In order to account for the total stainless steel mass needed for the pipes, the piping thickness is calculated for the 4 fluid solutions. It is assumed that the stainless steel density is 7500 kg/m^3.

Fluid	Thickness (mm)	Stainless Steel Mass (kg)
He	3.5	12
CO_2	7.1	185
Na	2	15.6
Molten Salt	2	29.66

Figure 18: Stainless Steel Mass Results

3.3 Full electric solution: Electric heating for the production of oxygen and hydrogen

Now that the fluidic heat transport solutions have been explored, the final section in this paper will be covering how the oxygen and hydrogen high temperature processes can be achieved electrically. In the past century, several electrical heating methods have been developed in the material industries. Some of the most common commercially used industrial heating methods include:

- Resistance heating (direct indirect)
- Infrared heating
- Induction heating
- Dielectric heating
- Microwave heating
- Radiofrequency heating
- Electric arc heating
- Plasma arc heating
- Electron-beam heating

In this trade study, direct resistive heating and microwave heating were the two methods analysed to reach oxygen production from lunar dust. Resistive heating produces oxygen from molten regolith electrolysis while microwave heating uses the hydrogen reduction of ilmenite to obtain oxygen. It was concluded that the microwave heating technology was favoured over the direct resistibe heating technology.

3.3.1 Direct heating molten regolith electrolysis

Direct resistive heating also known as Joule heating, requires the passage of an electrical current through a material, such as regolith, which heats up due its electrical resistivity. Microscopically, electrons colliding with the material lattice produce vibrations in the lattice which translate into an increase in temperature. Furthermore, oscillations of electron also tend to generate radiations, another important source of heat generation in the resistive heating process. The Joule heating of molten regolith allows for the electrolysis of the material. The electrolysis of regolith is a high temperature electrolytic process in which lunar regolith is dissolved in a molten oxide solvent through which a current is circulated thereby electrowinning liquid metal as a product and oxygen as a bi-product [10].

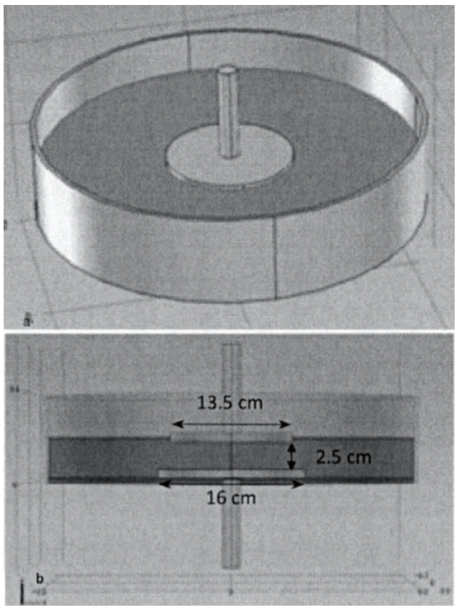

Figure 19: Schematic of a Joule-heated reactor [11]

As shown in 19, the reactor technology used for direct resistive heating consists of two electrode plates facing each other in a cylindrical steel shell closed at one end and containing the regolith. In this model taken from [11], the plates are made of iridium and are kept at a distance of 2.5cm from

each other. The upper electrode measures 13.5cm in diameter and acts as the anode where oxygen forms. It is immersed in the regolith at half of its 2.5cm thickness. The lower electrode, 16cm in diameter, acts as the cathode, where metals are formed and collected in molten form [11]. It is fully immersed in the regolith. Once a voltage is applied, an electrical current passes through the electrode plates and the regolith. The passage of this current through the regolith between the electrodes creates enough thermal energy to maintain the oxides and metals in molten form. All three processes of heat transfer (conduction, convection, radiation) contribute to the build up of heat during the reactor operation, with radiation playing an important role due to the high temperatures required to keep the materials molten. Similar technology revolving around high temperature electrolysis of oxides is used industrially in the production of Aluminium and Magnesium.

Despite this method being extremely advantageous when it comes to using regolith itself as the crucible material, there are several setbacks. The regolith must be in molten form to conduct electricity and regolith melting processes take place at temperatures as high as 1000^{o}C [11]. Therefore, a "cold start" to the reactor whereby only a voltage is applied between the electrode in an attempt to melt the regolith using Joule heating is not possible. Regolith is a granular material with extremely poor electrical and thermal conductivity at low temperatures. In fact, the thermal conductivity of the regolith is 0.02 W/Km at 25°C, a lower value than some of the best performing thermal insulation materials that have thermal conductivity between 0.035 and 0.16 W/Km [11]. In a NASA report [11], scientists attempted to apply voltages as high a 50V to cold start the reaction, but the Joule heating only generated a small 13^{o}C increment in temperature, from 25^{o}C to 38^{o}C using that voltage. Similarly, the electrical properties of regolith at low temperature indicate that no current can be circulated through to generate heat. The thermal conductivity of regolith increases substantially at higher temperatures though, reaching 3.8 W/Km at 1400^{o}C. Therefore, if resistive heating is to be used for oxygen production, the regolith must already be in molten phase, requiring a powerful external heating source to bring the material to at least a 1000^{o}C. One might achieve those conditions by concentrating solar beams on the regolith, requiring additional solar concentrators payload mass to be transported on the mission. The resistive heating method was set aside for this reason.

3.3.2 Microwave heating reduction of ilmenite

The hydrogen reduction of ilmenite involves reacting the ilmenite in a close container with hydrogen gas to separate water from the ilmenite reactant. This method was explored earlier in the fluidic transport solution of this trade study which can be found in equation (1). The reduction process contrasts directly with the Joule heated electrolysis of regolith, a fundamentally different process. Exploring an oxygen production mechanism that follows the same chemical reaction than the one shown in

equation (1) but with a different heating procedure allows to construct a very similar architecture to the one explored in Figure 10, replacing pipes with electrical cables for electric transport.

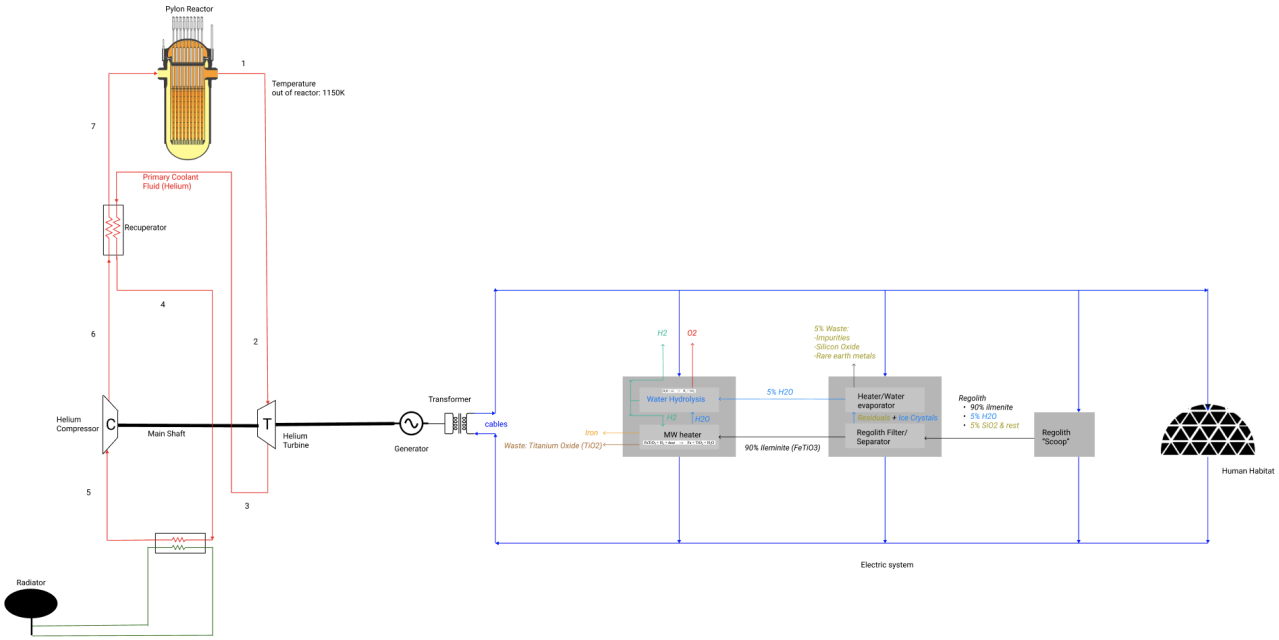

Figure 20: Full electric architecture for lunar base

Figure 20 illustrates what the full electric architecture would look like using power cables for electricity transport. The fluidized bed reactor from Figure 10 has been replaced by a microwave heated reactor facility to which a hydrogen streamline is connected.

Ilmenite is a dielectric material, and when subjected to microwave irradiation at a frequency above 1 GHz, the material will heat non-uniformly while its electrical properties are also modified. The resulting surface temperature of the ilmenite (T) is proportional to the irradiation time. In general, when electromagnetic waves are incident on a dielectric material, a part of the wave's energy is reflected, a part is absorbed, and a part is transmitted throughout the material. The quantity of energy absorbed is related to the frequency of the wave and the dielectric properties of the material. The impact of the radiation on the material is measured through the surface temperature which propagates through the rest of the material via diffusion. The response of any dielectric material to microwave irradiation can be explained in terms of the time dependence of the depolarizing current following the rapid removal of a steady polarising field [12]. This behaviour is governed by the dielectric constant ε, a frequency dependant quantity intrinsic to the material being irradiated as shown in equation (12).

$$\varepsilon(\omega) = \varepsilon'(\omega) + i\varepsilon''(\omega) \tag{12}$$

The imaginary part of the dielectric constant of ilmenite also known as the dielectric loss is written

in equation (13) [12].

$$\varepsilon'' = \varepsilon_0 + \frac{A}{\sqrt{2\pi}\omega_0 T} e^{-\frac{[ln(T/T_p)]^2}{2\omega_0^2}} \tag{13}$$

ε_0 and ω_0 are constants while T_p is a frequency independent peak temperature given as $T_p = 464 \pm 5K$.

The University of Johannesburg published a report [12] in which they studied the dielectric properties of ilmenite after subjecting some powder samples (18.7 g each) to 2.45 GHz microwave irradiation with 1 kW of power at room temperature (295^{o}K).

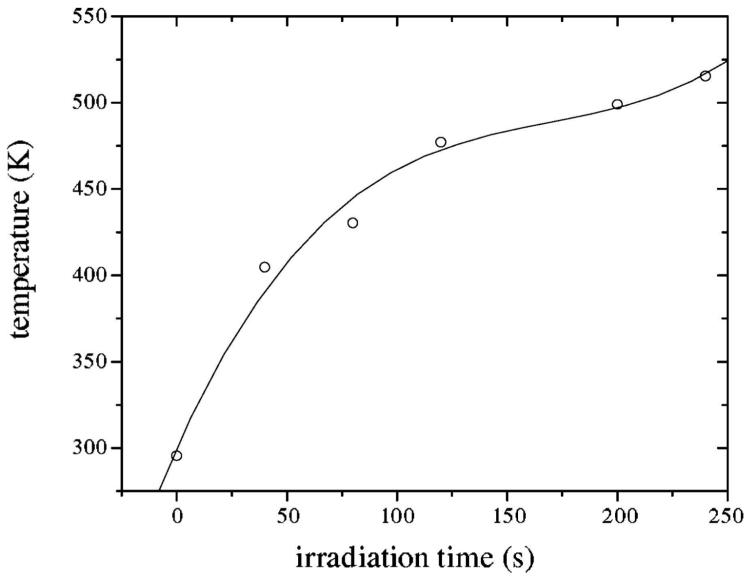

Figure 21: Variation of surface temperature with irradiation time for the ilmenite samples [12].

Figure 21 displays the relationship that was obtained experimentally between the surface temperature of ilmenite and the irradiation times when subjected to 1 kW microwave irradiation. A third order polynomial was fitted to the data and is shown in equation (14) [12].

$$T = 299.623 + 2.854t - 0.015t^2 + 3.028t^3 \tag{14}$$

Equation (14) demonstrates that the temperature is always increasing, given that the cubic term is positive. These results agree with former work carried by Wright et al [13]. A further study by L. A. Taylor and Meek [14] determined a relationship for the power deposited per unit volume by an electromagnetic field into a dielectric, which is displayed in equation (15).

$$P = KfE^2\varepsilon_r \tan\delta \tag{15}$$

where P is the power per unit volume; K is a constant; f is the frequency of radiation; E is electric field intensity; ε_r is the relative dielectric constant; and $\tan\delta\$$ is the loss tangent.

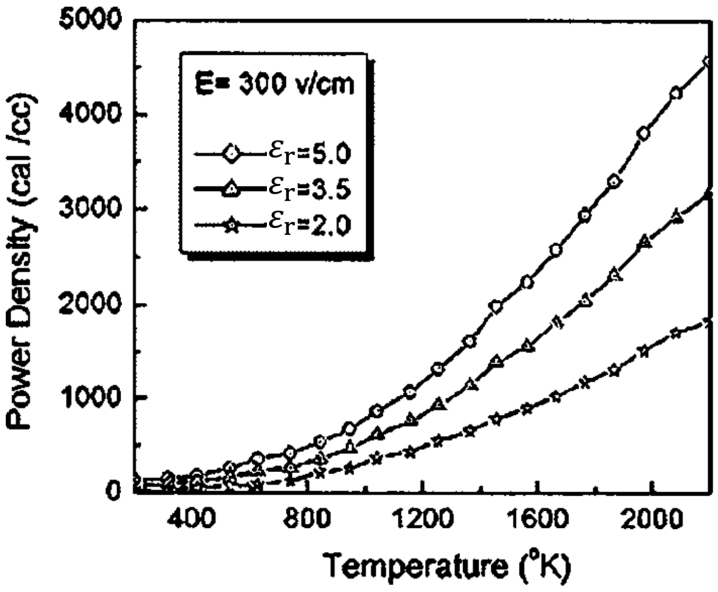

Figure 22: Calculated power density versus temperature coupled into lunar regolith using 2.45 GHz electro-magnetic radiation with E =300 V/cm and various values of ε_r[14].

Hence, Figure 22 shows that temperatures much higher than T=1273K (the threshold reaction temperature between ilmenite and hydrogen) can be reached using microwave heating.

3.4 Full Electric Solution: Power Transport with Cables

3.4.1 Cable Design

Electrical power transport will be achieved with cables. The cables analysed in this study are stranded copper conductors with 3:2 conductor redundancy, round cross-section, ETFE (Tefzel) insulation, filler rods, and an abrasion-resistant, thermal control jacket [15]. The redundancy allows the cable system to retain full functionality after one failure (fail-operate) while it would go into safe operating mode after a second failure that causes power to drop to 50% (fail-safe). In order to minimize the mass of the cables, electromagnetic interference shielding and armour against meteoroids was not included. Power connectors were included in the model, adding 1% to the total cable's mass in addition to data control communication wires which themselves added 5% cable mass fraction. With the cables, comes the power electronics, namely an AC source boost AC to AC frequency converter unit (AACU) and at the payload end of the cable, an AC cable buck AC to DC Rectifier (ACDU). Power electronics were designed with a 3:2 redundancy too, and protected by a carbon composite enclosure. Finally, a 50kg fixed mass was assumed for the cable spool and deployer mechanism based on a former NASA design. In this trade study, the lowest available cable cross section allowed was 1.291mm (16 AWG) with corresponding area of 1.31 mm^2. A minimum value was set to ensure structural robustness during deployment and operations.

Since the cables must be able to provide alternating current to a microwave heater, they must be able to transport AC electricity. The cables analysed in the NASA Lunar Surface-to-Surface Power Transfer report [15] operated at an AC frequency of 400Hz, cable operating temperature of 300K, which is consistent with the lunar south pole surface conditions, and electronics control temperature of 353K. The operational cooling of the cables electronics was performed by an Active Thermal Control System (ATCS) which was sometimes found to be a dominant contributor to the cable subsystem mass. The ATCS operated at a rejection temperature of 353K. The ATCS radiator is a two-sided planar heat rejection radiator with a specific mass of 6 kg/m^2. Finally a 5% system mass fraction was added to account for secondary structures and miscellaneous components in the cable assembly. The different cable subsystem elements of the NASA study are displayed in 23. All components, from wires and power electronics to radiators, were designed robust for long-duration, keeping in mind the lunar surface radiation and ground operations environments. Therefore, no degradation in efficiency was assumed for neither of the components.

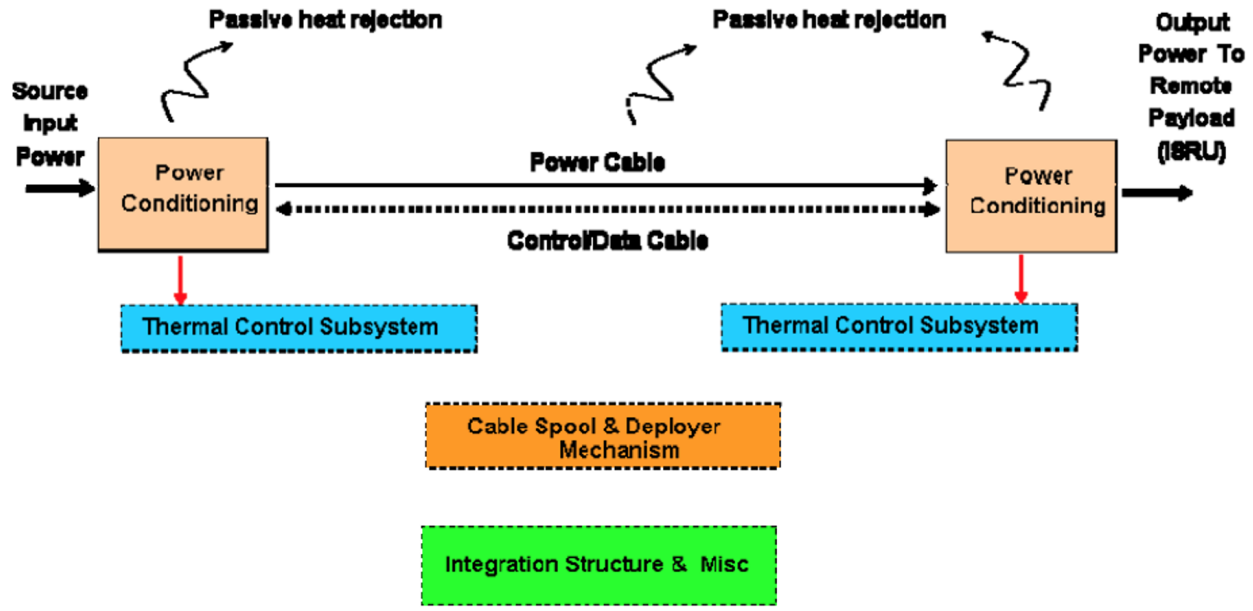

Figure 23: Cable power transfer subsystem elements

3.4.2 Cable subsystem deployment strategy

The power cables will be pre-integrated with the ISRU facility they need to support as it will allow for electrical verifications testing pre-launch and post landing on the lunar surface prior to deployment operations. The facility is first deployed to the desired site using keep-alive power provided by a dedicated battery accounted for in the payload. The EVA surface crew will then remove the payload from the Starship and install the integrated power cable assembly on the lunar rovers. While the

cables are still connected to the ISRU facility, the rovers then pull the assembly to the power source, making sure the cables remain flat on the ground. The cable routing factor in maintained under $\times 1.25$ during the deployment process and a routing path is selected to minimize cross-cable traffic which presents trip hazard to the EVA crew as well as cable damage hazard. Power and data connectors are mated to those of the power source electronics. Next, power electronics are activated, cable and conductor continuity is confirmed, systems functionality and control communications are verified to allow any issue to be troubleshooted before electricity transport begins. To allow power to flow, the up-steam and down-stream inhibits are removed, effectively closing the circuit. The power cables will be able to operate for 10 years without maintenance thanks to their 3:2 redundancy which provides fault tolerance.

3.4.3 Cable subsystem mass performance results

The control cabling mass (0.05kg/m) and power cable connector mass fraction (0.01) remained constant throughout the study. The mass of the cable subsystem is dependent on three key parameters: the power that flows through the cables, the voltage of the current flowing through the cables and the total length of cabling required to connect the infrastructures.

3.4.4 Power dependence of the cable subsystem

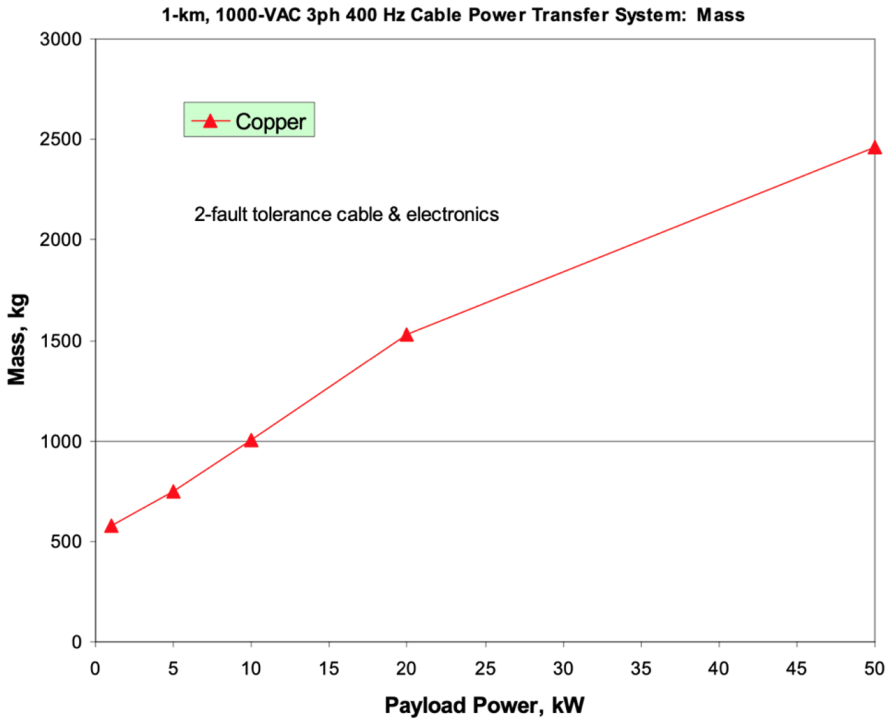

Figure 24: AC power cable subsystem mass versus payload power level

To analyse the power dependence, the length and voltage of the cable was fixed. As illustrated in 24. the subsystem mass for 1000m of cabling is essentially proportional to the payload power level. Power variations in the cables affect (1) the cable outer diameter (2) the Step-up ADCU TCS radiator plane area and (3) Step-down ADCU TCS radiator plane area. As a consequence, the mass of the following parameters are affected:

- Step up AACU mass, [kg]
- Power cable mass, [kg]
- Power cable connector mass, [kg]
- Step Down ADCU mass, [kg]
- Step up TCS (thermal control system) mass, [kg]
- Step down TCS (thermal control system) mass, [kg]
- Secondary structure (5%)

All mass parameters listed increase proportionally with an increase in power but the total subsystem mass is dominated by the cable mass item. By using the trend obtained in **??**, a relationship was established between payload power (P) and mass (m) for a 1000m subsystem of cabling.

$$m = 38.294P + 604.52 \tag{16}$$

Therefore, using equation (13) and extrapolating the data from 24, it was determined that 4434kg of payload mass would be required to transport 100kW of power through 1000m of cabling. It is interesting to note however, that the cable power transfer system's specific mass in [kg/kW] decreases as the power in the system increases as shown in Figure 3, in which a graph was plotted using data from [15]. The trendline follows a negative power relationship to the -0.63th.

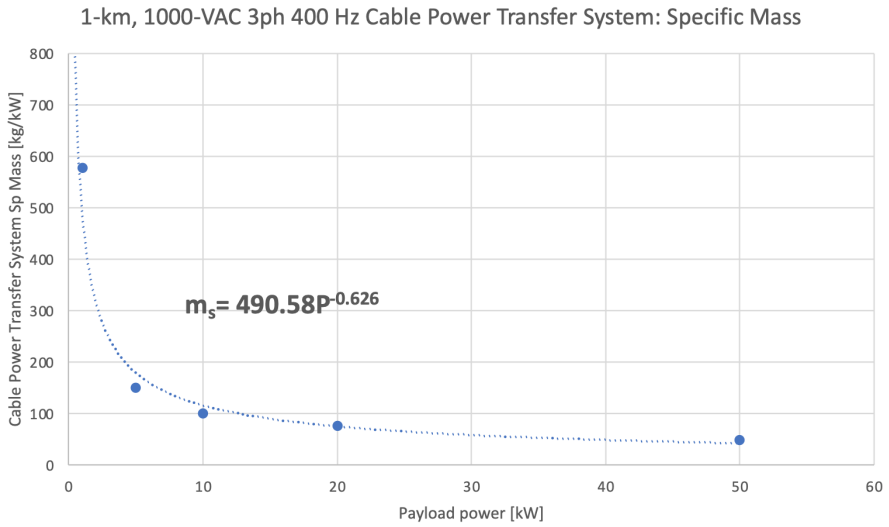

Figure 25: AC power cable subsystem specific mass versus payload power level

Length dependence of the cable subsystem: Furthermore, the relationship between the length and the mass of the subsystem is also analysed for cables fixed at 10kW of power. The results are demonstrated in 26

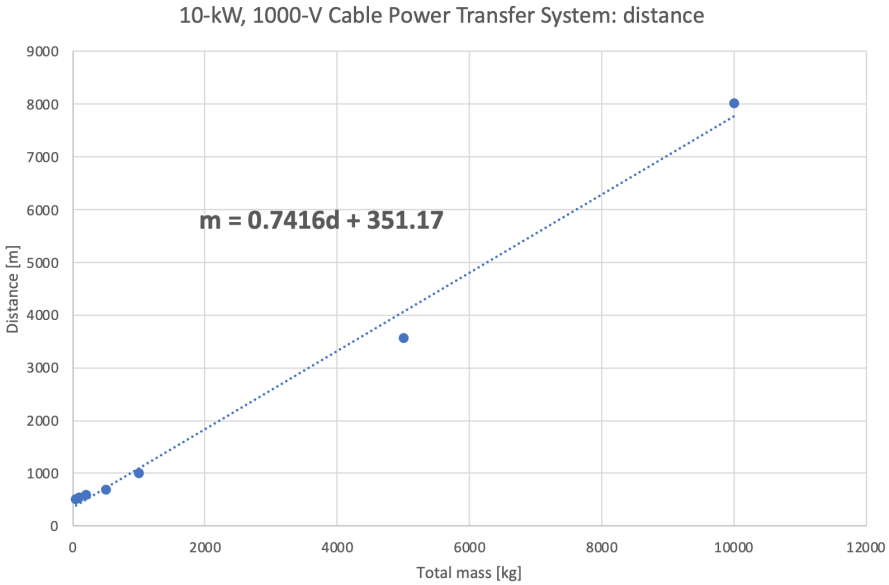

Figure 26: AC cable subsystem mass vs payload distance

The key reason behind the increase in mass this time, resides in (1) the increasing length of the system (the control cabling mass is constant for each data point at 0.05kg/m), (2) the Step-up AACU TCS radiator plane area (in m2) and (3) the cable outer diameter (cm). While the increase in (1) is simply caused by the added length that must be present to cover longer distances, (2) and (3)

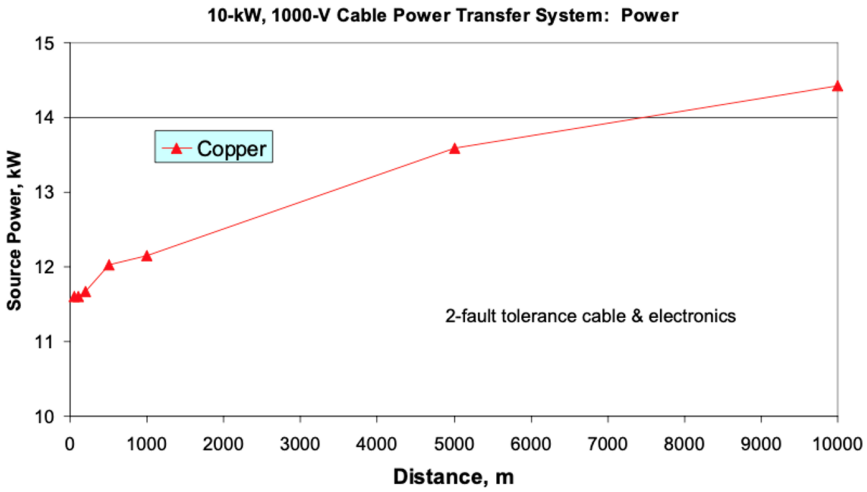

Figure 27: AC power cable subsystem source power versus payload distance

increase because of the conduction losses in the cables that occur as the electricity transport distance increases. This is directly demonstrated in 27. The cables analysed in this study were designed to deliver 10kW of power to a given infrastructure, but losses in the conduction process lead the power to decrease along the cables as a function of distance. In order to compensate for those losses, the source power must be increased thus increasing (2) and (3). This in turn, impacts the following mass parameters:

- Step up AACU mass [kg]
- Power cable mass [kg]
- power cable connector mass [kg]
- control cable mass [kg]
- Step up TCS mass [kg]
- secondary structure (5%)

These parameters all increase as a function of the subsystem length. It was concluded that source power growth was slightly less than proportional to cable length. Greater cable performance loss for longer length are accepted to reduce cable conductor mass. For shorter cable lengths ($\leq$500m), achieving a low subsystem mass requires heavier gauge cabling with lower performance loss to keep power electronics mass, the dominant mass item, lower [15].

Voltage dependence of the cable subsystem: Finally, the voltage is varied while the power and length of the cables were kept at 10kW and 1000m respectively.

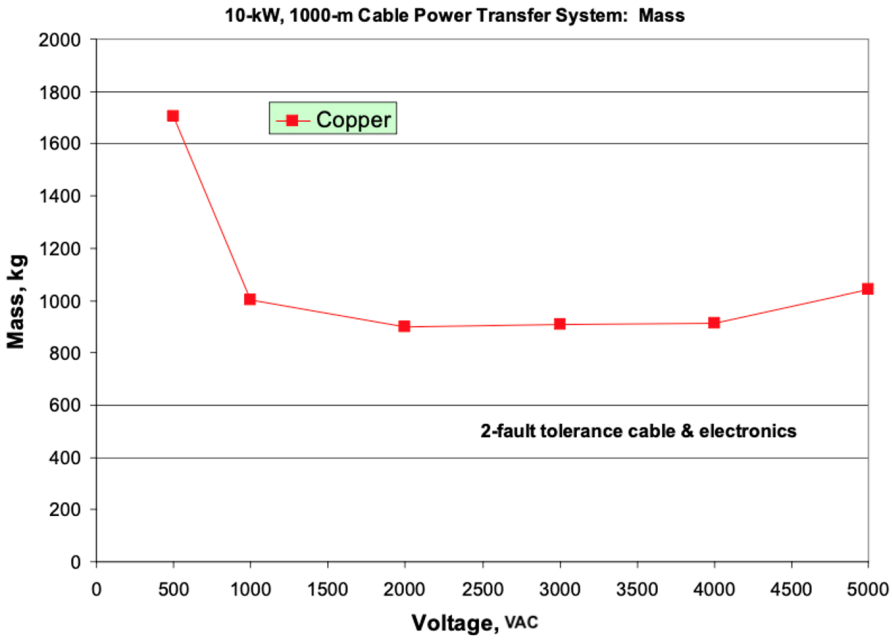

Figure 28: Mass versus AC cable operating voltage

A minimum in the mass is obtained for an AC voltage of 2000-VAC. This is an important number that will allow to limit the total payload capacity in the context of this trade study. The mass eventually stops decreasing because for voltages at or above 1000-VAC, the conductor minimum gauge size is reached. At this point, no further conductor mass savings can be achieved by increasing cable operating voltages. In fact, the cable outer diameter (cm) reaches a minimum of 0.94cm at 1000-VAC, and continues varying up and down in a step wise manner after that, never going below 0.94cm. On the other hand, at lower voltages, higher current levels require the use of larger conductor sizes. Those greatly increase the cable mass which dominates the subsystem mass.

The other reason voltage plays such a key part on cable mass is given by the dependence of Step-up AACU input power (in kW) on voltage. As voltage increases, the of Step-up AACU input power decreases proportionally. Consequently, the Step-up AACU TCS radiator plane area (m^2). The following mass parameters are impacted by the varying voltage:

- Step up AACU mass [kg].
- Power cable mass [kg].
- Power cable connector mass [kg].
- Step up TCS mass [kg].

4 Conclusion and Recommendations

Limitations and recommendations The greatest limitations in this trade study have been associated with the accessibility of data. Public thermodynamic data for molten salt and liquid sodium are scarce. Both materials need to be tested more at low pressures to understand their behavior in a lunar environment. Another limitation has been the lack of public technical information for commercial lunar technologies. Further the research is needed on the integration of lunar technologies with nuclear reactors, aiming to obtain a real understanding of power requirements and synergy between commercial operations. The main recommendation is to further the research on the analyzed technologies, including 3D multi physics simulation of the 4 chosen fluids in the lunar environment, radiation shielding from space and electric heating devices.

Conclusions Lunar technology research is anticipated to escalate in the near future. The proposed solutions should be addressed as a potential starting point for energy transfer between power generation and utilities. The Pylon 150 reactor, proposed by USNC, has the technical characteristics to provide heat and electricity for a small commercial lunar base in a safe, consistent and long lasting manner, while maintaining a small size.

Heat transfer from the reactor to the utilities proves itself to be one of the most important technological challenges to overcome in a lunar environment. The major difference when planning a system for the moon compared to planet earth lies in the compatibility with the outside temperatures and pressures. The study of the two thermal solutions result in a broad range of case studies to further analyze, as each system comes with a series of advantages and disadvantages.

Gas-cooled systems require high pressure environments, with peaks of 18.9 bar for helium and 13.42 bar for carbon dioxide, such systems are prone to pressure-based failures and leaks, but compensate with overall lower mass of coolant, that can be stored in low volume pressurized containers. Helium and carbon dioxide are also both considerably more inert than the liquid coolants chosen for the analysis, a characteristic that needs to be taken into account for material preservation of the systems.

The proposed liquid solutions analyze two innovative materials that are being investigated for advanced nuclear reactors. The reason why they were chosen was not only due to their great thermal characteristics, but also because, given the trends of nuclear and energy research, it is likely that system technologies that are paired with liquid sodium and molten chloride salts will be developed further and paired with lunar nuclear technologies. Both molten chloride and liquid sodium have the advantage of working at relatively low pressure, vastly reducing chances of failure for this reason. However, both fluids have a considerably higher density than the gases, and a greater mass of coolant will be required for lunar operations, increasing cost substantially at large scale. The other major disadvantage of these technologies lies in their corrosiveness, one of the major limitation of the

equivalent Gen IV reactor designs.

The electric heat transfer solutions show great potential for lunar applications, but require more technological investigations. A major drawback lies in the increase of electricity demand of the reactor, which would in turn require a bigger system overall, with more heat rejection through the use of more radiators or larger size ones. While an electric solution would not be able to recover any thermal energy from the nuclear reactor, energy system optimization on the moon is not as important as functionality and longevity, therefore these technologies have real potential to see implementation in the future.

References

[1] Christopher Morrison Wesley Deason Samuel Judd Vishal Patel Paolo Venneri Michael Eades Mark Reed. *THE PYLON: COMMERCIAL LEU NUCLEAR FISSION POWER FOR LUNAR, MARTIAN, AND DEEP SPACE APPLICATIONS*. Report P-5. USNC-Space, 2019.

[2] Anthony J. Colozza. *Small Lunar Base Camp and In Situ Resource Utilization Oxygen Production Facility Power System Comparison*. Report P-98. Nasa, 2020.

[3] A. J. Hanford. *Advanced Life Support Research and Technology Development Metric – Fiscal Year 2005, Revision A*. Report P-21. Jacobs Sverdrup, Houston, 2005.

[4] Jeffrey Hayden. *Air Revitalization System (ARS): Four-bed Molecular Sieve (4BMS)*. Report P-21. NASA, 2022.

[5] Colaprete. *Detection of Water in the LCROSS Ejecta Plume*. Report P-463. The Ohio State University, October 2010.

[6] Peter ; Heldmann Jennifer ; Wooden Diane ; Shirley Mark ; Ennico Kimberly ; Hermalyn Brendan ; Marshall William ; Ricco Antonio ; Elphic Richard C. ; Goldstein David ; Summy Dustin ; Bart Gwendolyn D. search by orcid ; Asphaug Erik ; Korycansky Don ; Landis David ; Sollitt Lukei Colaprete Anthony ; Schultz. *Detection of Water in the LCROSS Ejecta Plume*. Report P-346. Science, 2010.

[7] Jeffrey Hayden. *Evolutionary Space Communications Architectures for Human/Robotic Exploration and Science Missions*. Report P-21. The Ohio State University, 2004.

[8] L Fink J K; Leibowitz. *Thermodynamic and transport properties of sodium liquid and vapor*. Report P238. Argonne National Lab, 1995.

[9] Youyang Zhao. *Molten Chloride Thermophysical Properties, Chemical Optimization, and Purification*. Report P94. National Renewable Energy Laboratory, 2020.

[10] E. Carol. *Molten Regolith Electrolysis: The Extraction of Oxygen from Lunar Regolith*. Report P90. NASA, 2020.

[11] Laurent Sibille and Jesus A. Dominguez. *Joule-heated Molten Regolith Electrolysis Reactor Concepts for Oxygen and Metals Production on the Moon and Mars*. Report P90. NASA, 2007.

[12] A. F. MULABA-BAFUBIANDI C. CHITEME. *An investigation on electrical properties of microwave treated natural ilmenite (FeTiO3)*. Report P90. NASA, 2006.

[13] D. T. Vaniman R. D. Blake T. T. Meek R. A. Wright F. H. Cocks. *Thermal processing of ilmenite and titania-doped haematite using microwave energy*. Journal P90. 1989.

[14] Lawrence A. Taylor and Thomas T. Meek. *Microwave Sintering of Lunar Soil: Properties, Theory, and Practice*. Journal P90. July 2005.

[15] T. W. Kerslake. *Lunar Surface-to-Surface Power Transfer*. Report P90. NASA, 2007.

Appendix A Human Habitat Heat Losses: Term Definition

A_h surface area of the habitat (a hemisphere): $A_h = \frac{\pi d_h^2}{2}$.

d_h – habitat diameter: $d_h = 8$ [m].

ε_{hw} – habitat wall emissivity: $\varepsilon_{hw} = 0.07$.

ε_i – insulation emissivity: $\varepsilon_i = 0.07$.

n_l – number of layers of insulation: $n_l = 25.00$.

T_m– insulation temperature: $T_m = \left[\frac{\left(T_{hi}^2+T_{sn}^2\right)(T_{hi}+T_{sn})}{4}\right]^{\frac{1}{3}}$.

f_p – passthrough constant based on the presence of passthrough area.

A_{pt} of items such as wires or tubes that pass through the insulation: $f_p = 0.73 - 0.27A_{pt}$.

f_n – passthrough constant: $f_n = 4.547 - 0.501n_i$.

A_{pt} – passthrough area, given as a percentage: $A_{pt} = 1.00$.

n_{cp}– number of conductive paths.

k – thermal conductivity of the material.

A_{cp} – cross-sectional area of the material normal to the direction of the heat flow (conductive paths): $A_{cp} = \pi\left[\left(\frac{d_{icp}}{2} + t_{cp}\right)^2 - \left(\frac{d_{icp}}{2}\right)^2\right]$.

d_{icp} – the paths considered could be represented by a hollow cylinder shape with a specified inner diameter.

d_{cp} – Wall thickness.

L_{cp} – length of the conductive path.

f-friction factor

Appendix B Habitat Heat Loss formulae

Type of heat loss	**Equation**
Heat loss from the habitat through the insulation	$Q_i = \frac{A_h \sigma \left(T_{hi}^4 - T_{sn}^4\right)}{\left(\frac{1}{\varepsilon_{hw}}\right) + \left(\frac{2n_l}{\varepsilon_i}\right) - (n_l + 1)}$
Heat leak from passthroughs and seams in the insulation covering	$Q_{ps} = 0.644 \left(\frac{0.000136}{4\sigma T_m^2} + 0.000121 T_m^2\right) f_p f_n A_{h\sigma} \left(T_{hi}^4 - T_{sn}^4\right)$
Heat leak through conduction from the sources below	$Q_{cp} = \frac{n_{cp} k A_{cp} (T_{hi} - T_{sn})}{L_{cp}} = Q_{ra} + Q_{sl} + Q_{as}$
Heat leak from the habitat to the radiator	$Q_{ra} = \frac{n_{ra} k A_{ra} (T_{hi} - T_{sn})}{L_{ra}}$
Heat loss through the support legs	$Q_{sl} = \frac{n_{sl} k A_{sl} (T_{hi} - T_{sn})}{L_{sl}}$
Heat loss through the airlock structure	$Q_{sl} = \frac{n_{sl} k A_{sl} (T_{hi} - T_{sn})}{L_{sl}}$
Total	$Q_h = Q_i + Q_{ps} + Q_{ra} + Q_{sl} + Q_{as}$

Figure 29: Habitat Heat Loss

Appendix C Oxygen Production Electrical and Thermal Power

Electrical Power	P_{tO_2}
Scoop regolith	$P_{rs} = \frac{\mu_r d_{rs} M_r g}{3600 t_{sc} \eta_{em}}$
Transport regolith	$P_{rl} = \frac{(h_r + h_{rs}) M_r g}{3600 \eta_{em}} + 370 g_r$
Vibratory screener	$P_{vs} = \frac{0.45 M_r}{507.72 d_s + 49.91\sqrt{d_s}}$
Separate Regolith-Ilmenite	$P_{ms} = 0.196 n_{ri} M_r$
Lift Ilmenite	$P_{il} = \frac{(h_r + h_{rs}) M_r g}{3600 \eta_{em}} + 370 g_r$
Electrolyser	$P_e = G \frac{M_w}{\eta_e}$
Thermal Power	Q_{tO_2}
Heat Ilmenite	$Q_{hi} = \frac{\rho_i C_p (T_i - T_{io}) \pi d_r^2 h_r (1 - t_{rt} V_{ir})}{14400 t_h}$
Heat loss to surrounding	$Q_{ls} = \frac{\pi (d_r + n_l d_{il}) h_r \sigma (T_i^4 - T_{sd}^4)}{\frac{1}{\epsilon_{rO_2}} + \frac{2 n_l}{\epsilon_i} - n_l + 1}$
Power consumed in reaction	$Q_r = \frac{H_r \eta_s M_i}{3600}$

Table 4: Oxygen Production Electrical and Thermal Power